The Oxford Classic Links Epithelial-to-Mesenchymal Transition to Immunosuppression in Poor Prognosis Ovarian Cancers

Zhiyuan Hu[1,2], Paula Cunnea[3], Zhe Zhong[1,2,4], Haonan Lu[3,5], Oloruntoba I. Osagie[1,2], Leticia Campo[6], Mara Artibani[1,2,7], Katherine Nixon[3], Jennifer Ploski[3], Laura Santana Gonzalez[1,2], Abdulkhaliq Alsaadi[1,2], Nina Wietek[1,2], Stephen Damato[8], Sunanda Dhar[8], Sarah P. Blagden[6], Christopher Yau[9,10], Joanna Hester[11], Ashwag Albukhari[12], Eric O. Aboagye[5], Christina Fotopoulou[3], and Ahmed Ahmed[1,2]

ABSTRACT

Purpose: Using RNA sequencing, we recently developed the 52-gene–based Oxford classifier of carcinoma of the ovary (Oxford Classic, OxC) for molecular stratification of serous ovarian cancers (SOCs) based on the molecular profiles of their cell of origin in the fallopian tube epithelium. Here, we developed a 52-gene NanoString panel for the OxC to test the robustness of the classifier.

Experimental Design: We measured the expression of the 52 genes in an independent cohort of prospectively collected SOC samples ($n = 150$) from a homogenous cohort who were treated with maximal debulking surgery and chemotherapy. We performed data mining of published expression profiles of SOCs and validated the classifier results on tissue arrays comprising 137 SOCs.

Results: We found evidence of profound nongenetic heterogeneity in SOCs. Approximately 20% of SOCs were classified as epithelial-to-mesenchymal transition–high (EMT-high) tumors, which were associated with poor survival. This was independent of established prognostic factors, such as tumor stage, tumor grade, and residual disease after surgery (HR, 3.3; $P = 0.02$). Mining expression data of 593 patients revealed a significant association between the EMT scores of tumors and the estimated fraction of alternatively activated macrophages (M2; $P < 0.0001$), suggesting a mechanistic link between immunosuppression and poor prognosis in EMT-high tumors.

Conclusions: The OxC-defined EMT-high SOCs carry particularly poor prognosis independent of established clinical parameters. These tumors are associated with high frequency of immunosuppressive macrophages, suggesting a potential therapeutic target to improve clinical outcome.

[1]MRC Weatherall Institute of Molecular Medicine, University of Oxford, Oxford, England, United Kingdom. [2]Nuffield Department of Women's and Reproductive Health, University of Oxford, Oxford, England, United Kingdom. [3]Division of Cancer, Department of Surgery and Cancer, Imperial College London, England, United Kingdom. [4]School of Life Science, Peking University, Beijing, P.R. China. [5]Cancer Imaging Centre, Department of Surgery and Cancer, Faculty of Medicine, Imperial College London, London, England, United Kingdom. [6]Department of Oncology, University of Oxford, Oxford, England, United Kingdom. [7]Gene Regulatory Networks in Development and Disease Laboratory, MRC Weatherall Institute of Molecular Medicine, Radcliffe Department of Medicine, University of Oxford, Oxford, England, United Kingdom. [8]Department of Histopathology, Oxford University Hospitals, Oxford, England, United Kingdom. [9]Division of Informatics, Imaging and Data Sciences, Faculty of Biology Medicine and Health, The University of Manchester, Manchester, England, United Kingdom. [10]Alan Turing Institute, London, England, United Kingdom. [11]Transplantation Research and Immunology Group, Nuffield Department of Surgical Sciences, John Radcliffe Hospital, University of Oxford, Oxford, England, United Kingdom. [12]Department of Biochemistry, Faculty of Science, King Abdulaziz University, Jeddah, Saudi Arabia.

Note: Supplementary data for this article are available at Clinical Cancer Research Online (http://clincancerres.aacrjournals.org/).

Z. Hu and P. Cunnea contributed equally to this article.

C. Fotopoulou and A. Ahmed contributed equally as co-senior authors of this article.

Corresponding Authors: Ahmed Ahmed, WIMM, University of Oxford, Oxford, OX3 9DS, United Kingdom. Phone: 4401-8652-22820; E-mail: ahmed.ahmed@wrh.ox.ac.uk; and Christina Fotopoulou, Division of Cancer, Department of Surgery and Cancer, Imperial College London, W12 0NN, United Kingdom. E-mail: c.fotopoulou@imperial.ac.uk

Clin Cancer Res 2021;27:1570–9

doi: 10.1158/1078-0432.CCR-20-2782

Introduction

More than 90% of serous ovarian cancer (SOC) cases are high grade, a highly lethal gynecologic malignancy (1). The treatment regimen for high-grade SOC (HGSOC) consists of a combination of maximal effort debulking surgery and systemic anticancer cytotoxic and targeted agents. Recent advances support the use of PARP inhibitors for the treatment of HGSOCs, particularly those with BRCA1/2 mutations (2). However, the lack of robust and clinically reliable molecular classifications for non-BRCA1/2–mutated SOCs has hindered our ability to accurately predict patient prognosis or to introduce rationalized therapies. In contrast, clinically established molecular classification algorithms have been leveraged in other cancers in spite of inconsistencies in findings (3). Our approach is different in that our classification is driven by subtyping of the cell of origin. This approach avoids the heterogeneity introduced by genomic alterations in cancer and is, therefore, more likely to produce a stable classification.

In ovarian cancer, several attempts have been made to generate an accurate and clinically applicable molecular classification that correlated with prognosis. The seminal system developed by The Australian Ovarian Cancer Study (AOCS) is based on gene expression profiles, which identified a poor prognosis mesenchymal subtype, which was subsequently validated by The Cancer Genome Atlas (TCGA) study (4–6). This system relies on the clustering of transcriptomes and, thus, is apt to being disturbed by the noise of high-dimensional data. Another limitation of this classifier is the discrete readout, while the transcriptomic spectrum is likely continuous. Moreover, genomic profiling of ovarian cancers revealed seven molecular subtypes based on point mutations and structural aberrations that would likely confound tumor gene expression–based analysis (7, 8). Therefore,

Translational Relevance

Serous ovarian cancer is the most common histologic subtype of ovarian carcinoma. Because of substantial genetic heterogeneity, it has been challenging to develop robust prognostic classifications based on molecular stratification of high-grade serous ovarian cancer (HGSOC). We recently defined a gene panel "the Oxford Classic" (OxC) that robustly identifies a poor prognosis epithelial-to-mesenchymal transition–high (EMT-high) subtype of HGSOC. Here, we demonstrate that the NanoString-based OxC-derived high EMT scores are associated with poor prognosis in ovarian cancer independent of stage, grade, surgical outcome, or BRCA1/2 mutation status. These results demonstrate the clinical applicability of the OxC and its significant translational potential to enable future efforts for therapeutic optimization for EMT-high tumors.

the approach to stratify patients with HGSOC into molecular subtypes that associate with clinical outcome lacks robustness (9), likely owing to substantial intratumor genetic and nongenetic heterogeneity (10, 11). Recent advances in computational algorithms to deconvolute bulk tumors based on their DNA methylation (12, 13), DNA copy number (14), or RNA level profiles (15) are promising tools for molecular stratification. However, most expression-based deconvolution methods are limited by the requirement of prior knowledge of the number of tumor compartments and/or their gene expression profiles (16).

To address the aforementioned limitations, our recent work (17) developed a 52-gene panel termed the Oxford classifier of carcinoma of the ovary (Oxford Classic, OxC; **Fig. 1A**), which estimated the proportions of five molecular signatures [differentiated, KRT17, epithelial-to-mesenchymal transition (EMT), cell cycle, and ciliated] in each bulk tumor. The OxC was derived from single-cell RNA sequencing (RNA-seq) data of the normal fallopian tube epithelium (FTE), the putative site of origin of SOC (18), based on the hypothesis that the molecular subtypes of normal cell of origin could be reflected in the derived SOC subtypes. Thus, the first advantage of the OxC is that it is not confounded by the SOC genomic complexity. The conceptual basis of OxC is that any given tumor can be indicated by a mixture of these molecular signatures, which has been validated in our previous work. The percentage of each signature, that is, scores, can be estimated by a deconvolution algorithm (19). The robustness of the OxC prognostic correlation was demonstrated by our previous finding that tumors with high EMT scores (i.e., EMT-high tumors) were significantly associated with poor overall survival (OS) in seven independent and publicly available datasets, including TCGA (4) and the AOCS (6) datasets. Another advantage of OxC is the improved sensitivity for identifying the EMT-high subtype. Importantly, our recent work reported that the OxC-measured EMT scores identified a group of EMT-high tumors with poor prognosis that were previously defined as non-mesenchymal subtypes using previously reported classification models (17). A further advantage of the OxC is the dependence on only 52 genes. This can potentially lead to a more simplified and clinically feasible experimental procedure, which we will investigate in this work.

Another common reason for the failure of translation of molecular stratification of cancers to clinical application is the lack of homogeneity of the cohorts from which such stratifications are derived or subsequently tested. In ovarian cancer, a common source accounting for such lack of homogeneity is the variation in surgical practice and the biases introduced by suboptimal surgical quality, which inevitably makes the assessment of molecular classifications highly challenging. To overcome these biases, we aimed to validate our developed prognostic panel on a cohort of patients with SOC who had their surgery at a tertiary gynecologic cancer center that is recognized by the European Society of Gynaecological Oncology as Centre of Excellence for Ovarian Cancer Surgery with strictly applied criteria (20). This enabled us to significantly reduce the confounding effects of surgical practice variation on patients' survival.

NanoString (21) utilizes barcoding and imaging techniques to obtain absolute quantification of transcripts and enables customized measurement of selected genes. The application of NanoString on clinical samples has the advantage of requiring low input RNA with no amplification steps and this, therefore, ensures accuracy. We constructed a 52-gene NanoString panel to validate the robustness of the OxC (17) on an independent cohort of SOCs. We first tested the ability of the 52-gene panel to classify tumors into the five subtypes described previously. We further verified the association between EMT-high tumors and poor prognosis. Finally, we investigated the ability of the ciliated cell markers to distinguish low-grade SOCs and validated the results further using IHC.

Materials and Methods

Patient cohort

Patients included in the Hammersmith Hospital (HH) cohort were treated at Imperial College London NHS Trust, Hammersmith Hospital (London, England, United Kingdom), between June 2004 and October 2017. All procedures involving human participants were performed in accordance with the ethical standards of the institutional and/or national research committee and with the principles of the 1964 Declaration of Helsinki and its later amendments or comparable ethical standards. The project was performed under the Hammersmith and Queen Charlotte's and Chelsea Research Ethics Committee approval 05/QO406/178, and frozen tissues were supplied by the Imperial College Healthcare NHS Trust Tissue Bank, following full written informed patient consent. All methods were performed in accordance with the relevant guidelines and regulations. Patient demographics were collected retrospectively and are summarized in **Table 1**. Staging was defined according to Federation Internationale des Gynaecologistes et Obstetristes criteria for epithelial ovarian cancer (22). Patients were selected for this study according to the following criteria (i) diagnosis of SOC, (ii) patients were treated with primary cytoreductive surgery, (iii) patients had received platinum-based chemotherapy following primary surgery, and (iv) tumor samples were snap frozen and banked following primary surgery. Patients were excluded if they had a previous malignancy, had received neoadjuvant chemotherapy, or tumor tissues had low tumor cellularity. Tumor cellularity for tissues was reviewed by gynae-pathologists based in the West London Gynae Cancer Centre at Hammersmith Hospital, Imperial College Healthcare NHS Trust (London, England, United Kingdom).

Patients were evaluated at regular intervals following completion of their surgical and systemic treatment for evidence of disease recurrence. Clinical history, examination, and CA-125 (if the preoperative value was elevated) were performed every 3 months for the first 2 years and then 6 monthly. A CT/MRI scan was ordered if the above examinations revealed any pathology. An isolated elevation in CA-125 was not regarded as a recurrence.

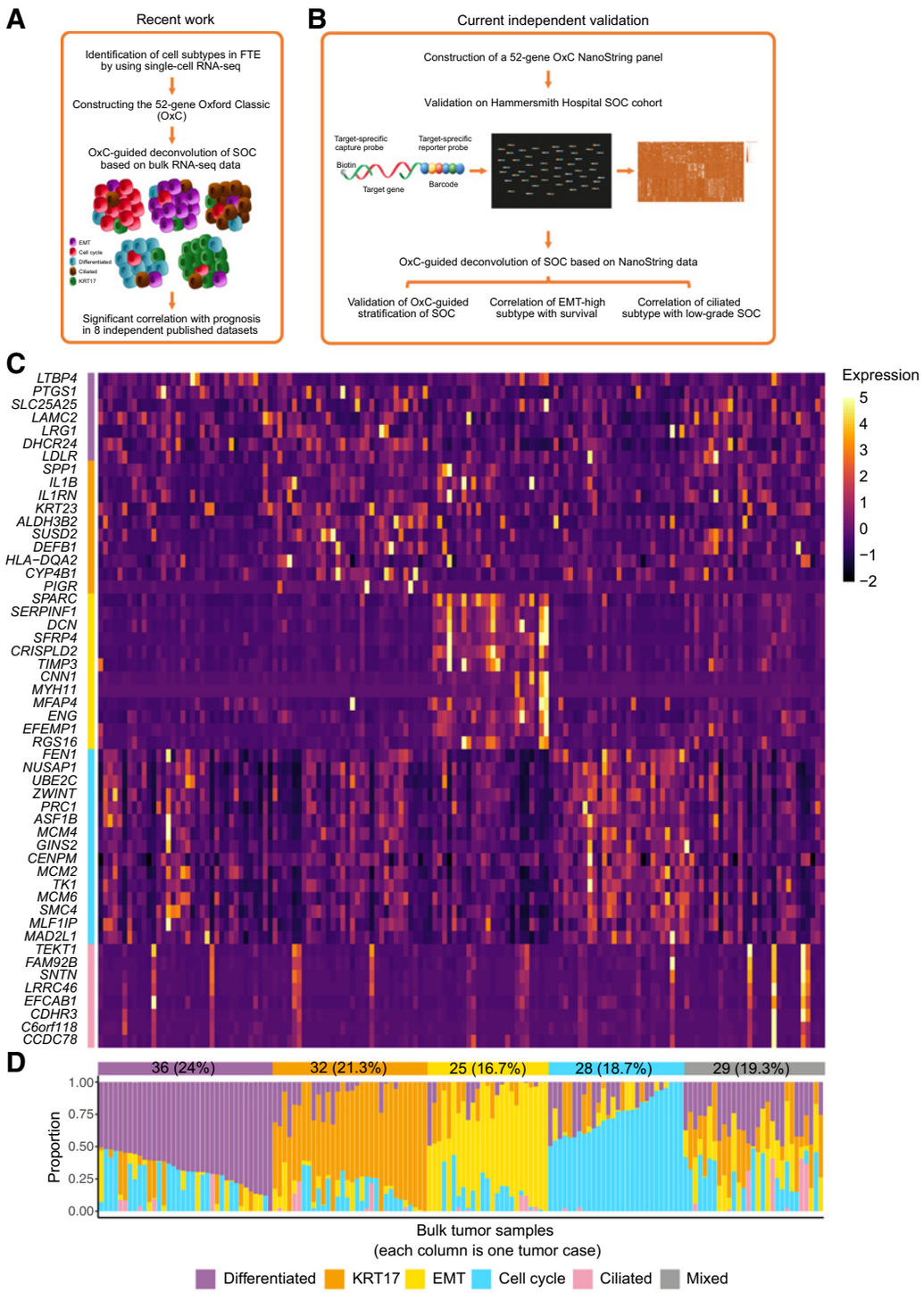

Figure 1.

Independent validation of OxC with NanoString assay in the HH cohort. **A,** Diagram shows the workflow of developing and validating OxC in our previous work. **B,** Diagram shows the workflow of an independent validation by performing NanoString OxC assay on the HH cohort. **C,** Heatmap shows the expression profiles measured by the NanoString OxC assay in 150 tumor samples. Each column is a tumor sample, and each row is a marker gene. The color represents the scaled expression levels. The vertical bar next to the gene names shows the signature each gene corresponds to. **D,** Stacked bar plot shows the deconvolution results of 150 tumor samples. Each column is a tumor sample corresponding to the one in **B**. The colors of bars represent the five signatures, and the size of each subbar denotes the proportion of a signature in a given tumor. The horizontal bar at the top shows the arbitrary discreet subtypes with the annotation of patient numbers and percentages.

Table 1. Summary of demographics and clinical characteristics of patients in the HH cohort.

Feature	All patients (150)	%	After exclusion (141)	%
Age (years)				
Median	60		60	
Range	18–90		18–90	
Stage				
I	8	5.3	8	5.7
II	12	8.0	12	8.5
III	90	60.0	84	59.6
IV	38	25.3	36	25.5
NA	2	1.3	1	0.7
Histologic subtype				
Serous	149	99.3	141	100.0
Endometrial serous carcinoma	1	0.7	0	0.0
Grade				
Low	7	4.0	6	4.3
High	125	83.3	117	83.0
NA	18	12.7	18	12.8
Biopsy site				
Abdominal wall	1	0.7	1	0.7
Omentum	17	11.3	17	12.1
Ovary	113	75.3	107	75.9
Peritoneum	1	0.7	1	0.7
Parametrium	1	0.7	1	0.7
Colon/bowel	3	2.0	3	2.1
Intra renal	1	0.7	1	0.7
Lymph node	1	0.7	1	0.7
Unspecified tumor mass	12	8.0	9	6.4
Postoperative residual disease				
Tumor free	110	73.3	106	75.2
Not tumor free	28	18.7	28	19.9
Unknown	12	8.0	7	5.0
BRCA status				
Wild-type	34	22.7	34	24.1
BRCA1 mutated	8	5.3	8	5.7
BRCA2 mutated	6	4.0	6	4.3
Unknown	102	68.0	93	66.0

RNA extraction

RNA was extracted from frozen tissues ($n = 150$) as described previously (23). A NanoDrop Spectrophotometer (Thermo Fisher Scientific) was used to measure RNA quality and the Qubit RNA HS Assay Kit (Invitrogen) was used to quantify RNA concentrations.

NanoString assay

The customized NanoString CodeSet, designed on the basis of the OxC (17), was purchased. The assay was performed following the manufacturer's manual for the nCounter XT CodeSet gene expression assays. For the hybridization step of each run, the solution containing 50 ng of total RNA and the master mix was incubated at 65°C for 19 hours. The hybridization solution was loaded into the nCounter SPRINT system. The raw data were processed by using the nSolver analysis software (RRID:SCR_003420) and following the manufacturer's protocol. All 150 samples passed the quality control incorporated in nSolver. The NanoString expression data were deposited at the Gene Expression Omnibus (GEO, RRID:SCR_005012; accession: GSE151335).

Analysis of NanoString data

The NanoString data were deconvolved as described previously (17). The reference matrix was composed of five transcriptomic signatures corresponding to four secretory cell states, namely differentiated, KRT17, cell cycle, and EMT, as well as the ciliated cell type. The proportions of the five signatures were estimated for each bulk tumor by using the R function downloaded from the CIBERSORT (RRID: SCR_016955) website (19). The reference matrix for the OxC has been reported previously (17). The estimated proportions were termed as scores. For each tumor, five scores added up to one.

Validation of NanoString readout by RNA-seq

To validate the correlation between NanoString and RNA-seq readout, we compared the NanoString data and the matched RNA-seq data from 10 HGSOC samples of the cases recruited under the Gynecological Oncology Targeted Therapy Study 01 (GO-Target-01, Ref #11/SC/0014) approved by South Central - Berkshire Research Ethics Committee and the Oxford Ovarian Cancer Predict Chemotherapy Response Trial (OXO-PCR-01, Ref 12/SC/0404) approved by the South Central Oxford C Research Ethics Committee. Both were conducted in accordance with Declaration of Helsinki. All participants involved in these study were appropriately informed and written informed consent was obtained. Tumor samples were biopsied during diagnostic laparoscopy or debulking surgery, immediately frozen on dry ice, and stored at −80°C. Frozen tumor samples were embedded in the optimal cutting temperature compound (NEG-50, Richard-Allan Scientific) and 10-μm-thick sections were taken using a CryoStar Cryostat Microtome (Thermo Fisher Scientific). RNA was extracted

from the section scrolls by using the RNeasy Mini Kit (Qiagen) according to the manufacturer's instructions. The libraries were prepared by using KAPA mRNA HyperPrep Kits (Roche) and sequenced on the NextSeq500 Platform (Illumina) using 75-bp pair-end reads. The RNA-seq data were trimmed by Trim Galore (RRID:SCR_011847), mapped to UCSC hg19 human genome assembly by STAR (RRID:SCR_015899; ref. 24), and counted by FeatureCount (25). RNA-seq data of the 10 OXO-PCR samples were deposited at GSE160085. The Pearson correlation coefficients and *P* values were calculated by R function cor.test.

Survival and association analysis

Two samples that were outliers in the deconvolution analysis (EMT scores ≥ 0.95), one sample that was an endometrial serous carcinoma subtype, and six samples with missing survival data were filtered out (Supplementary Fig. S1). We performed both uni- and multivariate survival analysis by using coxph function from R package, survival. *t* test was performed between the EMT scores and the residual disease. We could not perform association analysis with deconvolution results and BRCA status in HH cohort because of the limited number of patients with available BRCA status (**Tables 1**; Supplementary Table S1).

External data source and deconvolution analysis

TCGA "IlluminaHiSeq UNC" RNA-seq dataset (version: 2017-10-13) and AffyU133a array data (version: 2017-09–08) were downloaded from the UCSC Xena Data Hub (https://tcga.xenahubs.net; ref. 4, 26). The AOCS dataset was downloaded from the GEO (accession No. GSE9899). Seven microarray datasets were obtained from the R package, CuratedOvarianCancer (27–31). Exponential transformation was performed for the log-transformed data. The OxC scores of bulk tumors from the public datasets were calculated as describe previously (17). The immune cell proportions were estimated by applying the CIBERSORT algorithm to these RNA expression data in non-log linear space on the web-based platform using the published LM22 and LM6 signatures (19). The association analysis between the OxC signatures and immune signatures was performed by Pearson correlation test (function cor.test in R). The linear regression line was estimated by function lm and plotted by function ggplot2 (RRID:SCR_014601) in R.

BRCA1/2 mutation status analysis

For TCGA study (4), the matched data of BRCA status were downloaded from the cBioPortal (RRID:SCR_014555). We categorized samples with putative driver mutations, deep deletions, or both as BRCA1/2-mutated, and the ones with neither of those as BRCA1/2 wild-type. To investigate whether EMT-high tumors were enriched in a certain BRCA status, we performed *t* test between the EMT scores of BRCA1/2-mutated cases and BRCA1/2 wild-type cases by R function, t.test. To study the prognostic effect of BRCA status and EMT levels, we first performed multivariate survival analysis with continuous EMT scores, stages, and BRCA1/2 status. Samples were further dichotomized into EMT high and EMT low by the median, and survival analysis was conducted on four intersected groups: EMT-high BRCA1/2-mutated, EMT-high BRCA1/2 wild-type, EMT-low BRCA1/2-mutated, and EMT-low BRCA1/2 wild-type. To increase the power of this analysis, we repeated the analysis with 316 TCGA cases with clinical information (OS and stage), known BRCA1/2 status, and microarray data, which contained 70 BRCA1/2 wild-type and 246 BRCA1/2-mutated cases, while one case had missing stage information.

IHC

Calcyphosine (CAPS), a calcium-binding protein, is a marker of FTE ciliated cells, which we identified previously by single-cell RNA-seq and validated by IHC and immunofluorescence staining (17). To estimate the strength of the ciliated signature in HGSOC samples, we applied the IHC of CAPS on the sections of tumor samples. Formalin-fixed, paraffin-embedded tissue microarrays were cut into 2.5- or 4-μm sections. The Leica Bond Max Autostainer (Leica Microsystems) or Autostainer plus Link 48 (Dako) was used to automatically stain the tissue microarray sections with the anti-CAPS antibody (Sigma-Aldrich, catalog No. HPA043520; RRID:AB_10964138). Standard heat-induced epitope retrieval in retrieval buffer pH 6 was used. Tissue sections were kept at 100°C for 20 minutes, and then incubated with the primary antibody for up to 1 hour. The BOND Polymer Refine Detection System (DS9800, Leica Biosystems) was used to visualize the primary antibody. The stained slides were scanned by the ScanScope AT Digital Pathology Slide Scanner (Aperio) at 40× magnification.

Quantification of CAPS-positive cells

QuPath (32) was used to quantify the CAPS-positive cells. Tumor cells and stromal cells were manually selected on the basis of their nuclear morphology to train the machine learning algorithm incorporated in QuPath. After ensuring the fidelity of this algorithm, first we used it to classify cells into tumor and nontumor cells. The tumor cells were further classified as low (+), medium (++), and high (+++) based on the strength of the staining by the algorithm (Supplementary Table S2).

CAPS expression and tumor grades

A logistic regression model was built to predict the tumor grades using CAPS staining data:

$$\log\left(\frac{p(x)}{1-p(x)}\right) = \beta_0 + \beta_1 x_1 + \beta_2 x_2 + \beta_3 x_3$$

where, x is whether the tumor is low grade or high grade, and x_1, x_2, and x_3 represent the proportions of tumor cells expressing CAPS at the strength of low, medium, and high, respectively. $p(x)$ denotes the probability of x. The logistic regression model was trained with R function, glm. The ROC curve was calculated by R package, pROC (33). Each patient had one to four sections analyzed. The 141 low-grade tissue microarray samples were from 41 patients: two patients had one section per patient, four had two sections per patient, nine had three sections per patient, and 26 had four sections per patient. The statistical learning process was further performed using the 8-fold cross-validation, which evenly divided the data into eight portions and used one portion (1/8) as the testing set and the rest (7/8) as the training set per validation. This allowed us to test the variance of this model.

Availability of code

Scripts used to analyze and visualize the data were deposited in GitHub (https://github.com/OvarianCancerCell/oxford-classic-paper) and Code Ocean (https://codeocean.com/capsule/6646000).

Results

EMT scores correlate with poor survival in SOC

Previously, we demonstrated that the OxC RNA-seq–based scores correlate with SOC patient OS (17). To test the robustness of the results, we sought to (i) develop a gene panel using an independent

platform for measuring RNA expression and (ii) apply this panel on an independent SOC validation cohort. First, we constructed an OxC-based 52-gene panel using the NanoString platform and confirmed that this panel successfully passed all the required quality control measures. We confirmed that the NanoString readout was significantly correlated to the RNA-seq read counts in a small set of HGSOC samples for the OxC panel (Pearson $r = 0.89–0.95$; Supplementary Fig. S2). We next identified a cohort of 150 patients (**Table 1**) who had the following key features: (i) clinical data were prospectively collected, (ii) had proportionately homogenous disease stage (85.3% advanced stage III or IV), grade (83.3% high grade), and histopathology (149 SOCs), (iii) all had an attempt of maximum debulking surgery with 73.3% achieving no visible residual disease, and (iv) relatively long period of follow-up (median, ∼50.1 months; range, 0.1–153.7) and a high rate of events [73 patients (51%) died and 94 patients (70%) relapsed]. Patients had a median age of 61 (18–90) years. The BRCA status was available (somatic or germline) for only 32% of the patients. All patients postoperatively received at least four cycles of platinum-based chemotherapy. Median values of progression-free survival and OS were 18.2 (5.8–143.7) and 48.7 (0.1–153.7) months, respectively.

The expression level of the 52-gene NanoString panel was estimated from fresh-frozen tumor samples obtained from this cohort (**Fig. 1B** and **C**). Because RNA-seq–based OxC stratified SOCs into five molecular subtypes (differentiated, KRT17, EMT, cell cycle, and ciliated), we tested whether the new panel was able to reproduce this stratification in our cohort. In this cohort, 121 samples (80.7%) were stratified into one of these five subtypes, while 29 samples (19.3%) had a mixed phenotype (**Fig. 1D**). Notably, 16.7% of samples had the EMT-high phenotype. Univariate survival analysis showed that the EMT scores significantly correlated with poor survival and increased the hazard of death by 3.1-fold (**Table 2**). Accounting for other confounding variables was difficult because the relative homogeneity of the cohort meant that subgroups within the different variables were small. Nevertheless, multivariate analysis using established independent prognostic factors (stage, grade, and residual disease) revealed that the EMT scores independently associated with prognosis and increased the hazard of death by 3-fold (**Table 2**). Interestingly, neither grade nor residual disease was significantly associated with prognosis in this multivariate analysis. In addition, there was no significant correlation between EMT scores and residual disease status ($P = 0.40$ for all stages, and $P = 0.60$ for late-stage disease, Welch two-sample t test). However, this could be attributed to the homogeneity of the cohort resulting in small numbers of subgroups as mentioned earlier. Moreover, multivariate analysis showed that EMT scores were independently associated with progression-free survival ($P = 0.033$; HR, 2.5; $n = 111$; Supplementary Table S1), independent of stage, grade, and residual disease. Because of missing data, we were not able to assess the effect of BRCA1/2 mutation status as a potential confounder in this dataset. Therefore, we conducted an independent analysis on TCGA RNA-seq data and found that the EMT scores, or the scores of any other signature, were not associated with the BRCA1/2 mutation status (Supplementary Fig. S3A). The EMT score was significantly associated with survival, independent from BRCA1/2 mutation status and stage (EMT score: $P = 0.036$; HR, 2.1; Supplementary Table S3). In addition, examining the interaction between the two variables, revealed that the EMT-high BRCA1/2 wild-type group had the worst OS, independent from stage ($P = 0.0016$; HR, 1.8; Supplementary Fig. S3B). The results of microarray data with a larger sample size ($n = 315$) further confirmed these findings (Supplementary Fig. S3C; Supplementary Table S4). Taken together, these results support the idea that the OxC-based EMT scores independently correlated with poor prognosis in SOCs.

Table 2. Uni- and multivariate analysis for OS in the HH cohort.

Univariate analysis	Sample size	HR (95% CI)	*P*
EMT score (continuous)	141	3.091 (1.17–8.164)	**0.023**
Stage (III–IV vs. I–II)	140	2.626 (1.238–5.571)	**0.012**
Grade (low vs. high)	123	0.136 (0.019–0.988)	**0.049**
Residual disease (not tumor free vs. tumor free)	134	1.995 (1.158–3.439)	**0.013**

Multivariate analysis	Sample size	HR (95% CI)	*P*
EMT score (continuous)	116	2.991 (1.061–8.430)	**0.038**
Stage (III–IV vs. I–II)	116	2.635 (1.145–6.062)	**0.023**
Grade (low vs. high)	116	0.161 (0.022–1.178)	0.072
Residual disease (not tumor free vs. tumor free)	116	1.323 (0.736–2.378)	0.349

Note: The covariates of multivariate analysis are EMT score (continuous), stage (III–IV vs. I–II), grade (low vs. high), and residual disease (not tumor free vs. tumor free). $P < 0.05$ is highlighted in bold.

EMT scores are significantly associated with the abundance of M2 macrophages

Previous studies have highlighted the association between EMT in tumors and a poor immune response (34, 35). Therefore, we examined whether EMT-high scores correlated with features suggestive of an immunosuppressive environment in SOCs. To test this, we estimated the proportion of various immune cell signatures in TCGA data (4) using CIBERSORT (19) and correlated this with OxC-defined EMT-high tumors. We first used the LM6 reference matrix (19), which contained the transcriptomic signatures of six cell types, including CD8 T cells, CD4 T cells, B cells, neutrophils, natural killer cells, and monocytes, to deconvolve the RNA-seq data of TCGA cohort. The analysis revealed that EMT scores were positively correlated with the estimated proportions of the monocyte signature (Pearson $r = 0.25$; $P = 1.3e-05$; Pearson product-moment correlation test; Supplementary Fig. S4A). Tumors with higher EMT scores had significantly higher proportions of monocytes ($P = 8.021e-12$, one-sided Welch two-sample t test; **Fig. 2A**). To investigate which was the most prevalent monocyte subtype, we next conducted the analysis using the LM22 reference matrix (19), which can estimate the proportion of 22 types of immune cells in bulk tumors. Our results showed that EMT-high tumors had significantly higher proportions of M2 macrophages (ratio = 0.23/0.17; $P = 4.093e-05$, by one-sided Welch two-sample t test; **Fig. 2B**), but not of M0 or M1 macrophages, compared with EMT-low tumors (Supplementary Fig. S4B). Notably, all macrophage marker genes, except one, were upregulated in the EMT-high tumors (**Fig. 2C**). To test the robustness of the results, we repeated the analysis in a second independent dataset, the AOCS (6). This reproducibly showed that EMT-high tumors had significantly higher M2 macrophage proportions compared with EMT-low tumors ($P = 2e-05$, by one-sided Welch two-sample t test; **Fig. 2D** and **E**). Furthermore, the expression of the key EMT-high tumor marker gene, *SPARC* (17), significantly correlated with the expression of the M2 macrophage marker, *CD163* (36), in TCGA data and seven additional publicly available ovarian cancer expression datasets ($P < 0.05$; Supplementary Fig. S5). These results imply that the association between EMT-high scores and poor

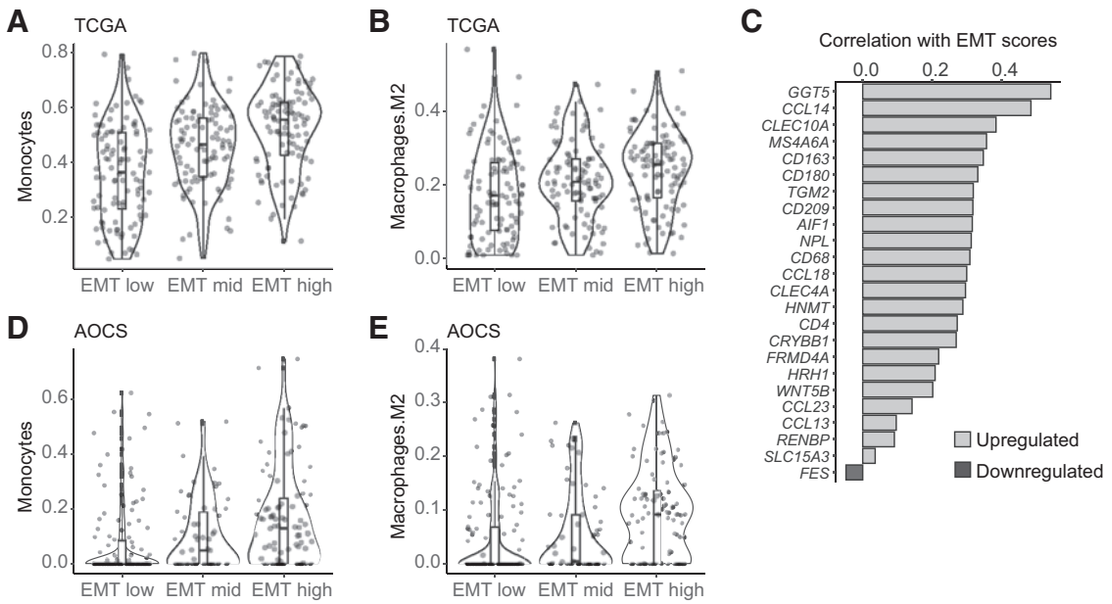

Figure 2.

EMT-high tumors have higher proportions of the macrophage M2 signature. **A,** Estimated proportions of monocytes in TCGA EMT-low, -mid, and -high tumors. EMT-high tumors tend to have higher proportions of monocytes (EMT high vs. EMT low; ratio = 0.52/0.36; P = 8.02e-12, by one-sided Welch two-sample t test). **B,** Estimated proportions of M2 macrophages in TCGA EMT-low, -mid, and -high tumors. EMT-high tumors tend to have higher proportions of M2 macrophages (ratio = 0.23/0.17; P = 4.09e-05, by one-sided Welch two-sample t test). **C,** The relationship between EMT scores and expression levels of putative macrophage M2 markers from the LM22 signature in TCGA data. **D,** The distribution of monocyte enrichment in EMT-low, -mid, and -high tumors in the AOCS data. Ratio = 0.17/0.07; P = 2.81e-05, by one-sided Welch two-sample t test. **E,** The distribution of M2 macrophage enrichment in EMT-low, -mid, and -high tumors in the AOCS data. Ratio = 0.10/0.05; P = 1.97e-05 by one-sided Welch two-sample t test.

survival may be, in part, due to the abundance of the immunosuppressive M2 macrophages.

Ciliated cell scores can efficiently predict the tumor grade of SOCs

An important feature of the OxC-based stratification is the association between the high-ciliated subtype scores and low-grade SOC (17). Therefore, we tested whether the new NanoString panel could reproduce these results.

In support of our recent findings, we found that the low-grade tumors had a significantly higher level of ciliated scores in the current cohort (**Fig. 3A**). We next hypothesized that the expression levels of ciliated markers can be used to predict the grade status of SOCs. To test this hypothesis, we first performed IHC for the ciliated marker, CAPS (17), on tissue microarrays of SOCs (n = 141 for low grade and n = 330 for high grade, from 137 patients; 1–4 data points per patient). We used automated analysis to quantify the level of CAPS staining into low, medium, and high using a machine learning algorithm (**Fig. 3B**; Supplementary Table S2; ref. 32). We next built a logistic regression model with the proportions of low, medium, and high cells as the independent variables and tumor grades as the response variables. This analysis revealed a strong significant association between CAPS expression level and tumor grade (coefficient = −10.72; P = 1.78e-10, logistic regression analysis). To test the predictive power of the model, we randomly selected 60% of the data to train the model and applied the parameters of the model on the remaining 40% of the data. The ROC curve showed that the CAPS expression level efficiently predicted the tumor grades (AUC ROC curve = 0.817; **Fig. 3C**; Supplementary Fig. S6). To confirm the results, we repeated the analysis by randomly sampling 60% of the data eight times and tested the predictive power of the obtained models on the remaining 40% of the data. This analysis indicated the stability of the predictive power of the model (AUC median, 0.82; range, 0.66–0.91; **Fig. 3D**). These results suggest that the expression of CAPS could be used to assist in determining the grade of SOCs.

Discussion

By taking advantage of the comprehensive characterization of FTE at a single-cell level, we previously developed the OxC and validated its prognostic power in eight independent ovarian cancer datasets. In this study, we were able to validate the OxC panel in an independent SOC cohort. Importantly, we were able to establish the significant prognostic value of the OxC-derived EMT scores and show that this was independent of other well-established prognostic factors, such as grade, stage, and postoperative residual disease. We identified approximately 20% of SOCs being classified as EMT-high tumors and hence associated with less favorable overall outcome. We hypothesize that these cases possibly correlate with the 20% of patients with advanced ovarian cancer that have been consistently shown to have poor prognosis despite optimal treatment and tumor-free surgical outcome (37, 38). EMT status could potentially become a valuable part of a future algorithm that will tailor surgical radicality and direct it to those who will benefit most.

EMT is defined by a transitional loss of the cellular epithelial phenotype and the acquisition of the cellular mesenchymal phenotype, which is related to poor prognosis in many cancer types. It has been established that EMT might directly lead to poor disease outcome by

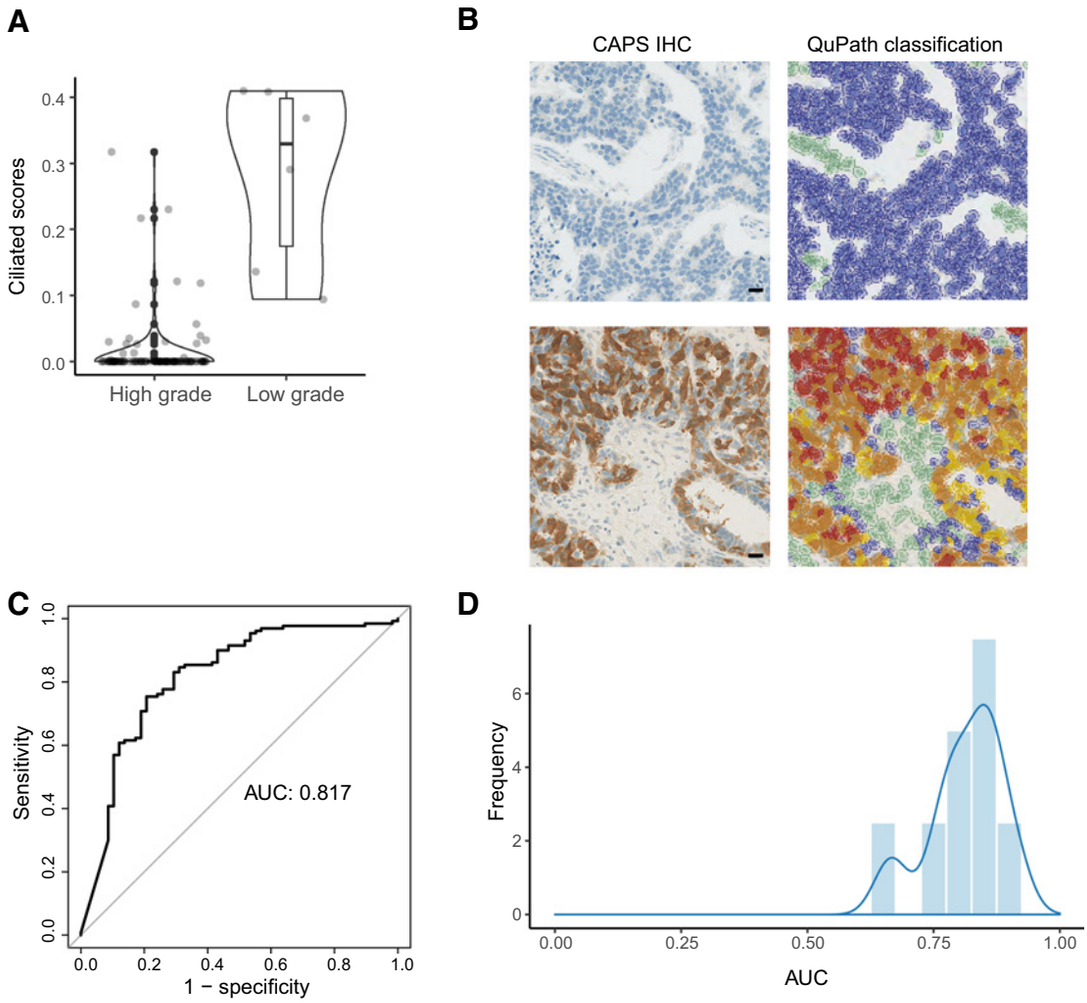

Figure 3.

Low-grade tumors tend to express higher levels of ciliated markers. **A,** Distribution of ciliated scores of low-grade ($n = 6$) and high-grade ($n = 116$) SOC in the HH cohort. Ratio = 0.28/0.1; $P = 0.0024$, by Welch two-sample t test. **B,** Examples depict the identification of CAPS-expressing tumor cells by QuPath. Green represents nontumor cells and blue denotes CAPS-negative tumor cells, while yellow, orange, and red denote the CAPS lowly expressing, moderately expressing, and highly expressing tumor cells, respectively (right). Scale bars, 20 μm. **C,** ROC curve of the logistic regression model that uses CAPS IHC data to predict tumor grades. AUC is shown in the figure. **D,** The distribution of AUC in the 8-fold cross-validation. The line represents the kernel density estimation.

facilitating tumorigenesis and metastasis (34). Similar to EMT, the abundance of intratumor macrophages has been reported previously to correlate with patient prognosis. While M1 macrophages exert tumoricidal effects, M2 macrophages possess immunosuppressive properties (39) and, thus, a high M1/M2 ratio seems to be translated into more favorable outcome (40), as opposed to high $CD163^{+}$ M2 macrophages, which correlate with elevated IL6 and IL10 with a shorter relapse-free survival (41). Besides, many studies have reported the relationship between macrophages and EMT, in which macrophages participate in EMT induction (42, 43). It is thought that mesenchymal-like tumor cells and macrophages can interact with each other in a paracrine fashion to form a positive feedback loop to facilitate tumor metastasis (44, 45). However, while the correlation between M2 macrophage abundance and poor prognosis has been reported (40, 41), the clinical significance of the link between EMT phenotype and macrophages has not been reported. This may have been due to the difficulty of accurately classifying EMT-high tumors. In addition, lower levels of tumor-infiltrating lymphocytes have been reported in cases of high levels of the EMT/mesenchymal component in HGSOC (4). Taken together, we hypothesize that the association between enriched EMT signatures and disease outcome might be mediated via an alternative or additional route, that is, the immunosuppressive effects of M2 macrophages (46). Although our study on clinical data could not unravel the causal relationship, we highlighted that the EMT and macrophage components are potentially key players in the immunosuppressive tumor microenvironment of HGSOC in humans. These putatively druggable components provide insights into development of therapies. While we envisage that the causal links among EMT, M2 macrophages, immunosuppression, and poor survival can be demonstrated by future work in animal models, our work

has highlighted potential immunotherapeutic strategies that can target macrophages in EMT-high SOCs. Our results show that the OxC-based EMT scores significantly correlate with the signature of M2 macrophages in SOCs, suggesting that the relationship and potential interactions between mesenchymal-like tumor cells and macrophages are clinically relevant.

Regarding the intriguing relationships between macrophages and molecular signatures derived from cell subtypes of origin, we hypothesized that cells in HGSOC "inherit" the cell plasticity from the normal cell of origin (17). Whether M2 macrophages induce the EMT state or the EMT state results in higher levels of M2 macrophages will be an important question to be addressed by future work, while the microenvironmental factors, for example, extracellular matrix, signaling ligands, metabolic products, or extracellular vesicles, may play an important in the interplay between the EMT signature and the macrophages in HGSOC. Among the 52 genes in the OxC panel, many genes in the OxC have been reported to have potential relationship with macrophages. Therefore, we envisage that future work can focus on characterizing the mechanistic links between OxC genes and macrophages.

In this work, we first reported the association between macrophages and EMT on the basis of the estimated proportions of macrophages using a deconvolution algorithm. Although deconvolution algorithms can efficiently exploit the existing bulk expression data, their accuracy is sometimes limited (47). More deconvolution methods are emerging with potential improvement in their performance (48, 49). Downstream validation using gene expression levels is still necessary. Therefore, we validated the deconvolution analysis by testing the correlation between EMT scores and individual genes that are used as markers for M2 macrophages. Reassuringly, we found a strong correlation at the individual gene level.

Our findings further confirm that low-grade SOCs express significantly higher levels of markers of ciliated FTE, including CAPS. This is consistent with the notion that low-grade tumors are more differentiated than high-grade tumors (50). This further validates the concept of classifying tumors based on the expression level of the normal cell of origin. Importantly, our work reported that IHC for CAPS expression can potentially assist the diagnosis of low-grade tumors. To our knowledge, this association has not been described previously. This finding has significant translational potential to assist in the diagnosis of low-grade tumors using established and readily available IHC and digital imaging methodology.

To summarize, in this study we validated the prognostic predictive power of OxC in an independent cohort of patients with SOC, using a 52-gene NanoString panel. By using a patient cohort with homogenous treatment quality, we endeavored to eliminate confounding bias that would interfere with evaluating the prognostic significance of OxC. These findings have important translational significance for the stratification of patients' care in SOC.

Authors' Disclosures

Z. Hu reports a patent for biomarkers in ovarian cancer pending. H. Lu reports grants from Qingzhen Biotech outside the submitted work. C. Yau reports a patent for biomarkers in ovarian cancer pending to A. Ahmed. J. Hester reports grants from Celgene-BMS outside the submitted work. E.O. Aboagye reports other from GE Healthcare outside the submitted work. C. Fotopoulou reports other from Roche, Sequana, Ethicon, and GlaxoSmithKline outside the submitted work. A. Ahmed reports personal fees and other from Singula Bio Ltd outside the submitted work, as well as has a patent for ovarian cancer biomarkers pending. No disclosures were reported by the other authors.

Disclaimer

The views expressed are those of the author(s) and not necessarily those of the NHS, the NIHR, or the Department of Health.

Authors' Contributions

Z. Hu: Conceptualization, data curation, software, formal analysis, supervision, funding acquisition, validation, investigation, visualization, methodology, writing-original draft, project administration, writing-review and editing. **P. Cunnea:** Data curation, software, funding acquisition, validation, investigation, methodology, writing-original draft, project administration, writing-review and editing. **Z. Zhong:** Formal analysis, investigation. **H. Lu:** Data curation, investigation. **O.I. Osagie:** Data curation, writing-original draft. **L. Campo:** Investigation. **M. Artibani:** Investigation. **K. Nixon:** Data curation, investigation. **J. Ploski:** Data curation, investigation. **L. Santana Gonzalez:** Investigation. **A. Alsaadi:** Investigation. **N. Wietek:** Investigation. **S. Damato:** Investigation. **S. Dhar:** Investigation. **S. Blagden:** Investigation. **C. Yau:** Investigation. **J. Hester:** Investigation. **A. Albukhari:** Investigation, visualization, writing-original draft. **E.O. Aboagye:** Data curation, investigation. **C. Fotopoulou:** Resources, software, supervision, funding acquisition, validation, investigation, methodology, writing-original draft, project administration, writing-review and editing. **A. Ahmed:** Conceptualization, resources, data curation, formal analysis, supervision, funding acquisition, validation, investigation, visualization, methodology, writing-original draft, project administration, writing-review and editing.

Acknowledgments

The research was supported by Ovarian Cancer Action (to A. Ahmed), the Cancer Research UK Oxford Centre (to A. Ahmed), Oxford Biomedical Research Centre (BRC), National Institute for Health Research (to A. Ahmed), and the National Institute for Health Research (NIHR) Biomedical Research Centre based at Imperial College Healthcare NHS Trust and Imperial College London. C. Fotopoulou and P. Cunnea were supported by the Myrovlytis Trust and Imperial Health Charity (to P. Cunnea). We acknowledge Ms. Nona Rama for help with tumor collection and Katherine Costello for clinical data collection. We acknowledge Dr. Mariolina Salio for her suggestions on macrophages. We acknowledge Professor Douglas A. Levine for his advice on BRCA data availability. Tissue samples were provided by the Imperial College Healthcare NHS Trust Tissue Bank. Other investigators may have received samples from these same tissues.

The costs of publication of this article were defrayed in part by the payment of page charges. This article must therefore be hereby marked *advertisement* in accordance with 18 U.S.C. Section 1734 solely to indicate this fact.

Received July 20, 2020; revised November 3, 2020; accepted December 23, 2020; published first January 14, 2021.

References

1. Siegel RL, Miller KD, Jemal A. Cancer statistics, 2020. CA Cancer J Clin 2020;70:7–30.
2. Lee J-M, Nair J, Zimmer A, Lipkowitz S, Annunziata CM, Merino MJ, et al. Prexasertib, a cell cycle checkpoint kinase 1 and 2 inhibitor, in BRCA wild-type recurrent high-grade serous ovarian cancer: a first-in-class proof-of-concept phase 2 study. Lancet Oncol 2018;19:207–15.
3. Sotiriou C, Pusztai L. Gene-expression signatures in breast cancer. N Engl J Med 2009;360:790–800.
4. Bell D, Berchuck A, Birrer M, Chien J, Cramer DW, Dao F, et al. Integrated genomic analyses of ovarian carcinoma. Nature 2011;474:609–15.
5. Wang C, Armasu SM, Kalli KR, Maurer MJ, Heinzen EP, Keeney GL, et al. Pooled clustering of high-grade serous ovarian cancer gene expression leads to novel consensus subtypes associated with survival and surgical outcomes. Clin Cancer Res 2017;23:4077–85.
6. Tothill RW, Tinker AV, George J, Brown R, Fox SB, Lade S, et al. Novel molecular subtypes of serous and endometrioid ovarian cancer linked to clinical outcome. Clin Cancer Res 2008;14:5198–208.
7. Wang YK, Bashashati A, Anglesio MS, Cochrane DR, Grewal DS, Ha G, et al. Genomic consequences of aberrant DNA repair mechanisms stratify ovarian cancer histotypes. Nat Genet 2017;49:856–65.

8. Macintyre G, Goranova TE, De Silva D, Ennis D, Piskorz AM, Eldridge M, et al. Copy number signatures and mutational processes in ovarian carcinoma. Nat Genet 2018;45:1127–270.
9. Chen GM, Kannan L, Geistlinger L, Kofia V, Safikhani Z, Gendoo DMA, et al. Consensus on molecular subtypes of high-grade serous ovarian cancer. Clin Cancer Res 2018;24:5037–47.
10. Bashashati A, Ha G, Tone A, Ding J, Prentice LM, Roth A, et al. Distinct evolutionary trajectories of primary high-grade serous ovarian cancers revealed through spatial mutational profiling. J Pathol 2013;231: 21–34.
11. Verhaak RGW, Tamayo P, Yang J-Y, Hubbard D, Zhang H, Creighton CJ, et al. Prognostically relevant gene signatures of high-grade serous ovarian cancer. J Clin Invest 2013;123:517–25.
12. Zheng X, Zhao Q, Wu H-J, Li W, Wang H, Meyer CA, et al. MethylPurify: tumor purity deconvolution and differential methylation detection from single tumor DNA methylomes. Genome Biol 2014;15:419–13.
13. Zheng X, Zhang N, Wu H-J, Wu H. Estimating and accounting for tumor purity in the analysis of DNA methylation data from cancer studies. Genome Biol 2017; 18:17.
14. Carter SL, Cibulskis K, Helman E, McKenna A, Shen H, Zack T, et al. Absolute quantification of somatic DNA alterations in human cancer. Nat Biotechnol 2012;30:413–21.
15. Gong T, Szustakowski JD. DeconRNASeq: a statistical framework for deconvolution of heterogeneous tissue samples based on mRNA-Seq data. Bioinformatics 2013;29:1083–5.
16. Yadav VK, De S. An assessment of computational methods for estimating purity and clonality using genomic data derived from heterogeneous tumor tissue samples. Brief Bioinformatics 2015;16:232–41.
17. Hu Z, Artibani M, Alsaadi A, Wietek N, Morotti M, Shi T, et al. The repertoire of serous ovarian cancer non-genetic heterogeneity revealed by single-cell sequencing of normal fallopian tube epithelial cells. Cancer Cell 2020;37:226–7.
18. Labidi-Galy SI, Papp E, Hallberg D, Niknafs N, Adleff V, Noe M, et al. High grade serous ovarian cancers originate in the fallopian tube. Nat Commun 2017;8:1093.
19. Newman AM, Liu CL, Green MR, Gentles AJ, Feng W, Xu Y, et al. Robust enumeration of cell subsets from tissue expression profiles. Nat Methods 2015; 12:453–7.
20. Fotopoulou C, Concin N, Planchamp F, Morice P, Vergote I, Bois du A, et al. Quality indicators for advanced ovarian cancer surgery from the European Society of Gynaecological Oncology (ESGO): 2020 update. Int J Gynecol Cancer 2020;30:436–40.
21. Geiss GK, Bumgarner RE, Birditt B, Dahl T, Dowidar N, Dunaway DL, et al. Direct multiplexed measurement of gene expression with color-coded probe pairs. Nat Biotechnol 2008;26:317–25.
22. Prat J, FIGO Committee on Gynecologic Oncology. Staging classification for cancer of the ovary, fallopian tube, and peritoneum. Int J Gynaecol Obstet 2014; 124:1–5.
23. Lu H, Arshad M, Thornton A, Avesani G, Cunnea P, Curry E, et al. A mathematical-descriptor of tumor-mesoscopic-structure from computed-tomography images annotates prognostic- and molecular-phenotypes of epithelial ovarian cancer. Nat Commun 2019;10:764.
24. Dobin A, Davis CA, Schlesinger F, Drenkow J, Zaleski C, Jha S, et al. STAR: ultrafast universal RNA-seq aligner. Bioinformatics 2013;29:15–21.
25. Liao Y, Smyth GK, Shi W. featureCounts: an efficient general purpose program for assigning sequence reads to genomic features. Bioinformatics 2014;30:923–30.
26. Goldman M, Craft B, Hastie M, Repečka K, McDade F, Kamath A, et al. The UCSC Xena platform for public and private cancer genomics data visualization and interpretation. bioRxiv 2019;326470. doi: https://doi.org/10.1101/326470.
27. Ganzfried BF, Riester M, Haibe-Kains B, Risch T, Tyekucheva S, Jazic I, et al. curatedOvarianData: clinically annotated data for the ovarian cancer transcriptome. Database 2013;2013:bat013.
28. Bentink S, Haibe-Kains B, Risch T, Fan J-B, Hirsch MS, Holton K, et al. Angiogenic mRNA and microRNA gene expression signature predicts a novel subtype of serous ovarian cancer. PLoS One 2012;7:e30269.
29. Pils D, Hager G, Tong D, Aust S, Heinze G, Kohl M, et al. Validating the impact of a molecular subtype in ovarian cancer on outcomes: a study of the OVCAD Consortium. Cancer Sci 2012;103:1334–41.
30. Bonome T, Levine DA, Shih J, Randonovich M, Pise-Masison CA, Bogomolniy F, et al. A gene signature predicting for survival in suboptimally debulked patients with ovarian cancer. Cancer Res 2008;68:5478–86.
31. Crijns APG, Fehrmann RSN, de Jong S, Gerbens F, Meersma GJ, Klip HG, et al. Survival-related profile, pathways, and transcription factors in ovarian cancer. PLoS Med 2009;6:e24.
32. Bankhead P, Loughrey MB, Fernández JA, Dombrowski Y, McArt DG, Dunne PD, et al. QuPath: open source software for digital pathology image analysis. Sci Rep 2017;7:16878–7.
33. Robin X, Turck N, Hainard A, Tiberti N, Lisacek F, Sanchez J-C, et al. pROC: an open-source package for R and S+ to analyze and compare ROC curves. BMC Bioinformatics 2011;12:77–8.
34. Shibue T, Weinberg RA. EMT, CSCs, and drug resistance: the mechanistic link and clinical implications. Nat Rev Clin Oncol 2017;14:611–29.
35. Voon DC, Huang RY, Jackson RA, Thiery JP. The EMT spectrum and therapeutic opportunities. Mol Oncol 2017;11:878–91.
36. Lau SK, Chu PG, Weiss LM. CD163: a specific marker of macrophages in paraffin-embedded tissue samples. Am J Clin Pathol 2004;122:794–801.
37. Harter P, Sehouli J, Lorusso D, Reuss A, Vergote I, Marth C, et al. A randomized trial of lymphadenectomy in patients with advanced ovarian neoplasms. N Engl J Med 2019;380:822–32.
38. Bois du A, Reuss A, Pujade-Lauraine E, Harter P, Ray-Coquard I, Pfisterer J. Role of surgical outcome as prognostic factor in advanced epithelial ovarian cancer: a combined exploratory analysis of 3 prospectively randomized phase 3 multicenter trials: by the Arbeitsgemeinschaft Gynaekologische Onkologie Studiengruppe Ovarialkarzinom (AGO-OVAR) and the Groupe d"Investigateurs Nationaux Pour les Etudes des Cancers de l"Ovaire (GINECO). Cancer 2009;115: 1234–44.
39. Krishnan V, Schaar B, Tallapragada S, Dorigo O. Tumor associated macrophages in gynecologic cancers. Gynecol Oncol 2018;149:205–13.
40. Zhang M, He Y, Sun X, Li Q, Wang W, Zhao A, et al. A high M1/M2 ratio of tumor-associated macrophages is associated with extended survival in ovarian cancer patients. J Ovarian Res 2014;7:19–16.
41. Reinartz S, Schumann T, Finkernagel F, Wortmann A, Jansen JM, Meissner W, et al. Mixed-polarization phenotype of ascites-associated macrophages in human ovarian carcinoma: correlation of CD163 expression, cytokine levels and early relapse. Int J Cancer 2014;134:32–42.
42. Nieto MA, Huang RY-J, Jackson RA, Thiery JP. EMT: 2016. Cell 2016;166:21–45.
43. Robinson BD, Sica GL, Liu Y-F, Rohan TE, Gertler FB, Condeelis JS, et al. Tumor microenvironment of metastasis in human breast carcinoma: a potential prognostic marker linked to hematogenous dissemination. Clin Cancer Res 2009;15: 2433–41.
44. Wyckoff J, Wang W, Lin EY, Wang Y, Pixley F, Stanley ER, et al. A paracrine loop between tumor cells and macrophages is required for tumor cell migration in mammary tumors. Cancer Res 2004;64:7022–9.
45. Su S, Liu Q, Chen J, Chen J, Chen F, He C, et al. A positive feedback loop between mesenchymal-like cancer cells and macrophages is essential to breast cancer metastasis. Cancer Cell 2014;25:605–20.
46. Peranzoni E, Lemoine J, Vimeux L, Feuillet V, Barrin S, Kantari-Mimoun C, et al. Macrophages impede CD8 T cells from reaching tumor cells and limit the efficacy of anti-PD-1 treatment. Proc Natl Acad Sci U S A 2018;115:E4041–50.
47. Sturm G, Finotello F, Petitprez F, Zhang JD, Baumbach J, Fridman WH, et al. Comprehensive evaluation of transcriptome-based cell-type quantification methods for immuno-oncology. Bioinformatics 2019;35:i436–45.
48. Peng XL, Moffitt RA, Torphy RJ, Volmar KE, Yeh JJ. *De novo* compartment deconvolution and weight estimation of tumor samples using DECODER. Nat Commun 2019;10:4729–11.
49. Wang L, Sebra RP, Sfakianos JP, Allette K, Wang W, Yoo S, et al. A reference profile-free deconvolution method to infer cancer cell-intrinsic subtypes and tumor-type-specific stromal profiles. Genome Med 2020;12:24–22.
50. Diaz-Padilla I, Malpica AL, Minig L, Chiva LM, Gershenson DM, Gonzalez-Martin A. Ovarian low-grade serous carcinoma: a comprehensive update. Gynecol Oncol 2012;126:279–85.